

9

Intraplate earthquakes induced by reactivation of buried ancient rift system along the eastern margin of the Japan Sea

AITARO KATO

Abstract

Utilizing a dense seismic network deployed immediately after recent large intraplate earthquakes along the eastern margin of the Japan Sea, we discovered that stepwise and tilted block structures of the basement, which are geophysical evidence of a Miocene rift system formed during the spreading of the Japan Sea, are widely distributed beneath the thick sedimentary basin in the Niigata region. A similar structure associated with the ancient rift system is imaged in the source area of the Noto-Hanto earthquake. Most aftershocks following the recent intraplate earthquakes align roughly along the tilted block boundaries of the basement and are controlled by weaknesses associated with buried rift systems. Furthermore, we discuss the stress loading mechanisms for source faults of intraplate earthquakes. The structural coincidence between the stress axis distribution and the velocity structure observed in the Niigata region raises the possibility that ductile deformation of the sediments can partially accumulate elastic strain in the brittle parts of the fault zone. In addition, low-velocity anomalies are localized beneath the seismogenic zones, indicating that fluids may have locally weakened the crust. This study therefore suggests that reactivation of pre-existing faults within ancient rift systems by stress loading through ductile flow in the upper crust and creeping of the locally weakened lower crust is a plausible mechanical explanation for intraplate earthquakes.

9.1 Introduction

Many intraplate earthquakes have occurred in the Japanese islands as a result of internal deformations of overlying plates. The Japanese islands are situated in a tectonically active zone, where two oceanic plates are subducting (Figure 9.1a). Beneath northeast Japan, the Pacific plate is subducting from the east through the Japan Trench at a convergence rate

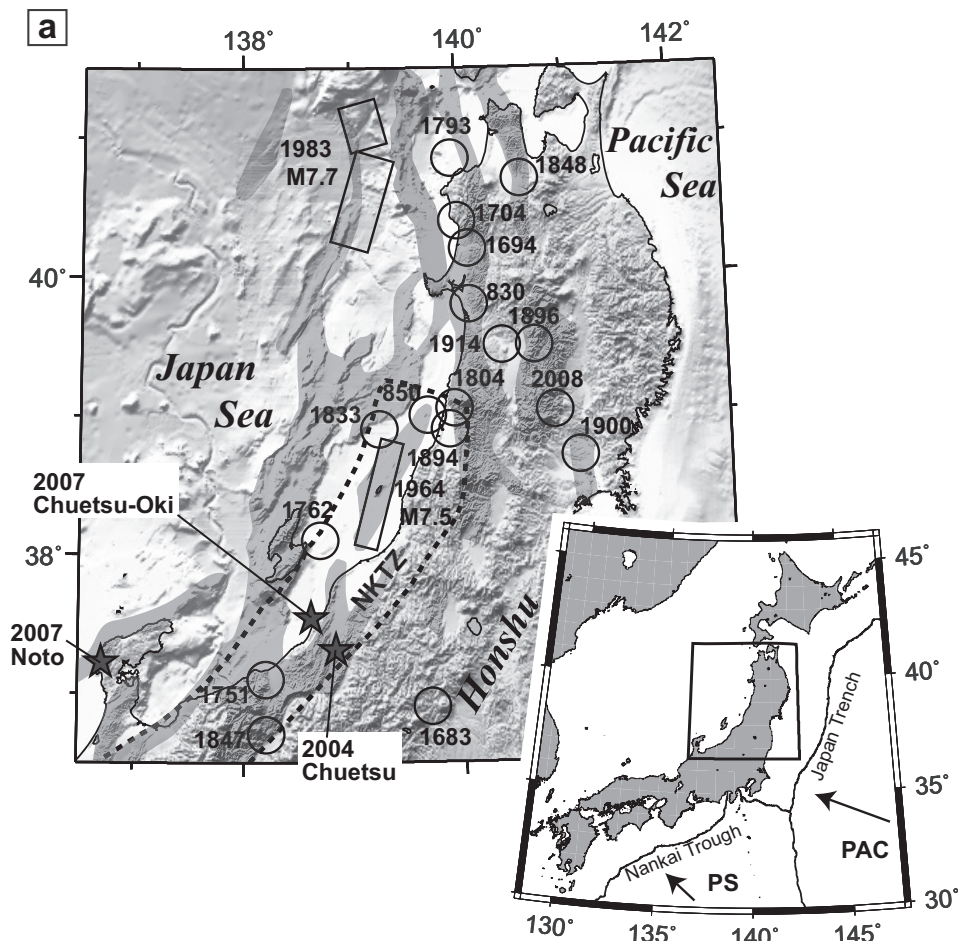


Figure 9.1 Seismotectonic setting in northern Honshu, Japan (modified after Kato *et al.*, 2009). (a) The Niigata–Kobe Tectonic Zone (NKTZ) is outlined by the broken line and contractional zones based on geological studies are drawn as gray-shade zones (Okamura *et al.* (2007)). Fault locations of recent major earthquakes and epicenters of historical large earthquakes with a magnitude greater than 7.0 are plotted as rectangles and circles, respectively (Usami, 2003). Three stars denote the epicenters of the 2004 Niigata-ken Chuetsu earthquake, the 2007 Chuetsu-Oki earthquake and the 2007 Noto-Hanto earthquake. The inset shows the location of the studied area (black framed rectangle). PAC, Pacific plate; PSP, Philippine Sea plate.

of ~ 8.5 cm/yr, whereas beneath southwest Japan, the Philippine Sea plate is subducting from the southeast through the Nankai Trough at a convergence rate of $\sim 2\text{--}5$ cm/yr (e.g., Loveless and Meade, 2010). Due to subduction of the two oceanic lithospheres, intraplate earthquakes in the Japanese islands are more frequent than in other regions in the world. Damage caused by the intraplate earthquakes is usually devastating due to their shallow depths (less than 15 km).

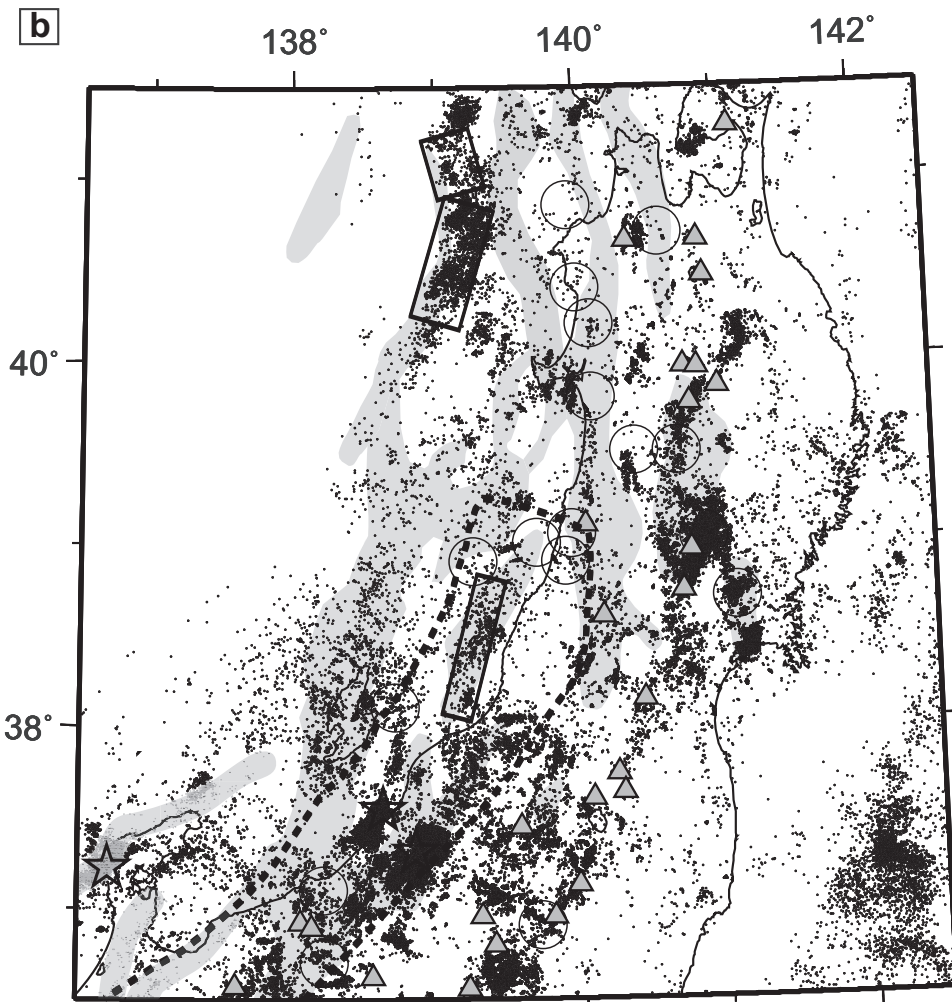


Figure 9.1 (b) Map of epicenters with magnitude greater than 1.0 reported by the JMA for the period from 2000 to 2010. Triangles denote locations of active volcanoes. Other symbols are the same as in (a).

Particularly in the eastern margin of the Japan Sea, historical and recent destructive intraplate earthquakes (e.g., the 1964 Niigata earthquake with Japan Meteorological Agency (JMA) magnitude (M_{JMA}) 7.5; the 1983 Japan Sea earthquake with M_{JMA} 7.7) have been concentrated along a zone of high east–west contractional strain rates detected by geodetic measurements (larger than 10^{-7} per year) and geological studies (Sagiya *et al.*, 2000; Okamura *et al.*, 2007) (Figure 9.1a). In addition, shallow microseismicity revealed by a state of the art nationwide high-sensitivity seismic network (e.g., Obara *et al.*, 2005) has been intensive along this contractional zone (shaded area in Figure 9.1b). Within the

contractional zone, three destructive intraplate earthquakes showing reverse faulting with a strike of approximately N35°E most recently occurred in the Niigata and Noto-Hanto regions. In addition, a shallow intraplate earthquake with M_{JMA} 6.7 was induced by the 2011 M_w 9.0 Tohoku-Oki earthquake at the south portion of this contractional zone.

These earthquakes are commonly located within Miocene–Pleistocene sedimentary basins. These sedimentary basins were formed as back-arc basins in a rift structure that developed during the opening stage of the Japan Sea (25–15 Ma) (Sato *et al.*, 1994). Several normal faults have subsequently been inverted as reverse faults owing to a change in the tectonic stress regime from extension to compression since 3.5 Ma. This stress inversion led to well-developed thrusts and related surface folding. The overlap between intraplate earthquakes and ancient rift systems beneath thick sediments suggests that ancient rift systems are important for nucleating present-day intraplate earthquakes in the compressional inverted basins. However, the details of the ancient buried rift structures and their potential effects on the seismogenesis of large intraplate earthquakes have not been fully understood. In addition, the driving force behind the generation of intraplate earthquakes (loading mechanism) remains a subject of controversy (e.g., Iio *et al.*, 2002, 2004). It has been argued that local heterogeneities in crustal structure play an important role in controlling the spatiotemporal evolution of seismicity and associated faulting behavior (e.g., Michael and Eberhart-Phillips, 1991; Chiarabba *et al.*, 2009; Kato *et al.*, 2009, 2010a; Zhao *et al.*, 2011). In order to illuminate these issues, it is thus critical to fully describe the crustal heterogeneity originating in the ancient rift system. Seismic tomography combined with a dense seismic network are powerful tools for imaging high-resolution crustal structures as well as precise hypocenters, and offer new insights into potential seismogenic structures. The dense and well-covered ray-paths from the many aftershocks triggered by each large earthquake provide us precious opportunities to (1) investigate the regional velocity structure and stress field in detail with a spatial resolution of ~3–5 km, and (2) demonstrate that crustal heterogeneities associated with the Miocene rift structures significantly contribute to present-day seismogenesis along the eastern margin of the Japan Sea.

9.2 Data and method

Permanent seismic networks have been operated on the Japanese islands by the National Research Institute for Earth Science and Disaster Prevention (NIED), the Japan Meteorological Agency (JMA), and various universities. Nevertheless, the average spacing of these stations (from 20 to 30 km) is insufficient for resolving the detailed velocity structures in the source regions of inland earthquakes with magnitude less than 7.0. In order to obtain high-resolution three-dimensional seismic velocity tomographic images in source regions, as well as precise hypocenters, we have deployed a series of temporary dense seismic stations interpolating between the existing stations of the permanent seismic network. Recent technical advancement of portable seismometers and data acquisition systems has enabled us to carry out quick deployment of a dense seismic network for durations longer than 3 months. We usually deploy the temporary seismic stations with spatial intervals of several kilometers.

Each temporary seismic station continuously records three-component waveform signals at the sampling rate of 200 or 100 samples/second. Each station is equipped with a GPS receiver, which maintains the accuracy of the internal clock. After retrieving the waveforms, we then merge the huge earthquake datasets recorded by the temporary seismic network together with the corresponding data from permanent stations in each target region. We then manually pick P- and S-wave arrival times from earthquake waveforms detected based on the JMA catalog. We determine high-resolution three-dimensional velocity structures as well as precise hypocenters, applying the double-difference tomography method (Zhang and Thurber, 2003) to both the arrival time data and the differential arrival times obtained by the manually picked and waveform correlation method (e.g., Kato *et al.*, 2006a). In addition, we analyze high-resolution stress fields using focal mechanisms determined by the polarity data of P-wave first motion.

9.3 The 2004 Niigata-ken Chuetsu and 2007 Chuetsu-Oki earthquakes

Two neighboring destructive intraplate earthquakes (both with M_{JMA} 6.8) showing reverse faulting with a strike of approximately N35°E recently occurred in the Niigata region: the first, Niigata-ken Chuetsu earthquake on October 23, 2004, and the second, Niigata-ken Chuetsu-Oki earthquake on July 16, 2007 (Figure 9.1). The focal areas of the 2004 Chuetsu and 2007 Chuetsu-Oki earthquakes were located within a thick (locally >6 km deep) deformed Miocene–Pleistocene sedimentary basin (the Niigata Basin), which is characterized by NNE–SSW-trending faults and anticlinal fold hinges that form topographic hills (Figure 9.2a). This sedimentary basin was formed as a back-arc basin in a rift structure that developed during the opening stage of the Japan Sea (25–15 Ma). This basin is bounded to the east by the Shibata-Koide Tectonic Line (SKTL), where basement rocks dating back to more than 30 Ma are widely exposed. Geological studies (e.g., Sato, 1994) have inferred that parts of the normal faults within the rift system have subsequently been reactivated as a reverse fault system since the extensional tectonic stress regime changed to a compressional one in the late Pliocene (2–3 Ma), through a process of compressional inversion (Williams *et al.*, 1989). Although these shallow large earthquakes generated many fissures and landslides on the surface, only minor surface faulting was observed (Maruyama *et al.*, 2005).

We conducted a series of temporary seismic observations through a dense deployment of 145 portable stations after the 2004 earthquake (from October to November, 2004) (Kato *et al.*, 2006a, 2007) and 108 portable stations including a linear-seismic array on land and 20 ocean-bottom seismometers after the 2007 earthquake (from July to August, 2007) (Kato *et al.*, 2008a, 2009; Shinohara *et al.*, 2008) (Figure 9.2a).

9.3.1 Aftershock distribution and dynamic rupture process

Depth sections of P-wave velocity (V_p) models along W35°N–E35°S lines are shown in Figure 9.2b. Relocated aftershocks (gray circles) distributed within ±2.5 km of each line

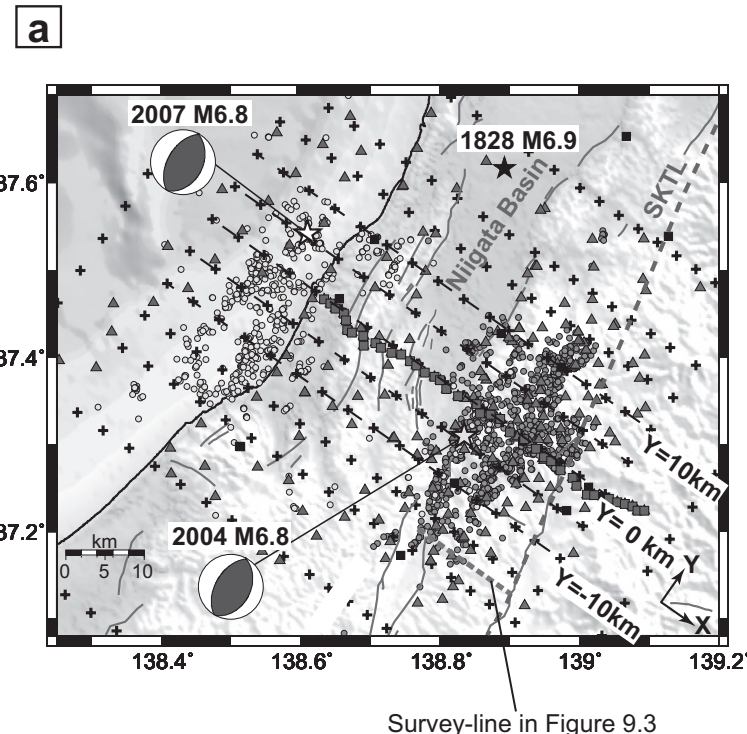


Figure 9.2 Dense seismic observations and regional V_p model in the Niigata region (modified after Kato *et al.*, 2009). (a) Map of relocated aftershocks of the 2004 Chuetsu and the 2007 Chuetsu-Oki earthquakes (gray circles observed in 2004, and yellow circles in 2007). Moment tensors for the two earthquakes are from the NIED. Blue squares denote the linear seismic array, and red and blue triangles represent temporary stations deployed after the earthquakes in 2004 and 2007, respectively. Black squares denote permanent stations. The grid used in the tomography analysis is plotted with crosses, and horizontal dashed lines correspond to the cross-sections in Figure 9.2b. Major active faults are drawn as red lines; a blue broken line indicates the SKTL. The gray broken line denotes a seismic survey line shown in Figure 9.3.

are superimposed. The striking aspect of the relocated aftershocks is a multi-segmented and complex distribution. The aftershock distributions associated with the 2004 mainshock reveal that the mainshock and the largest aftershock (A1) occurred on two 60° northwestward (NW) dipping planes, located approximately 5 km apart. Conversely, the October 27 event (A2) occurred on a southeast-ward (SE) dipping plane with a dip angle of 25° that was conjugate to the mainshock fault plane (Kato *et al.*, 2006a, 2009).

Similar conjugate sets of fault planes are also imaged in the aftershock sequences following the 2007 Chuetsu-Oki earthquake (e.g., Kato *et al.*, 2008a) (Figure 9.2b). From the center to the southern area, most of the aftershocks aligned along a SE-dipping plane with a low dip angle. Conversely, aftershocks in the north aligned along both NW- and SE-dipping planes. These planes were virtually normal to each other or conjugate. The

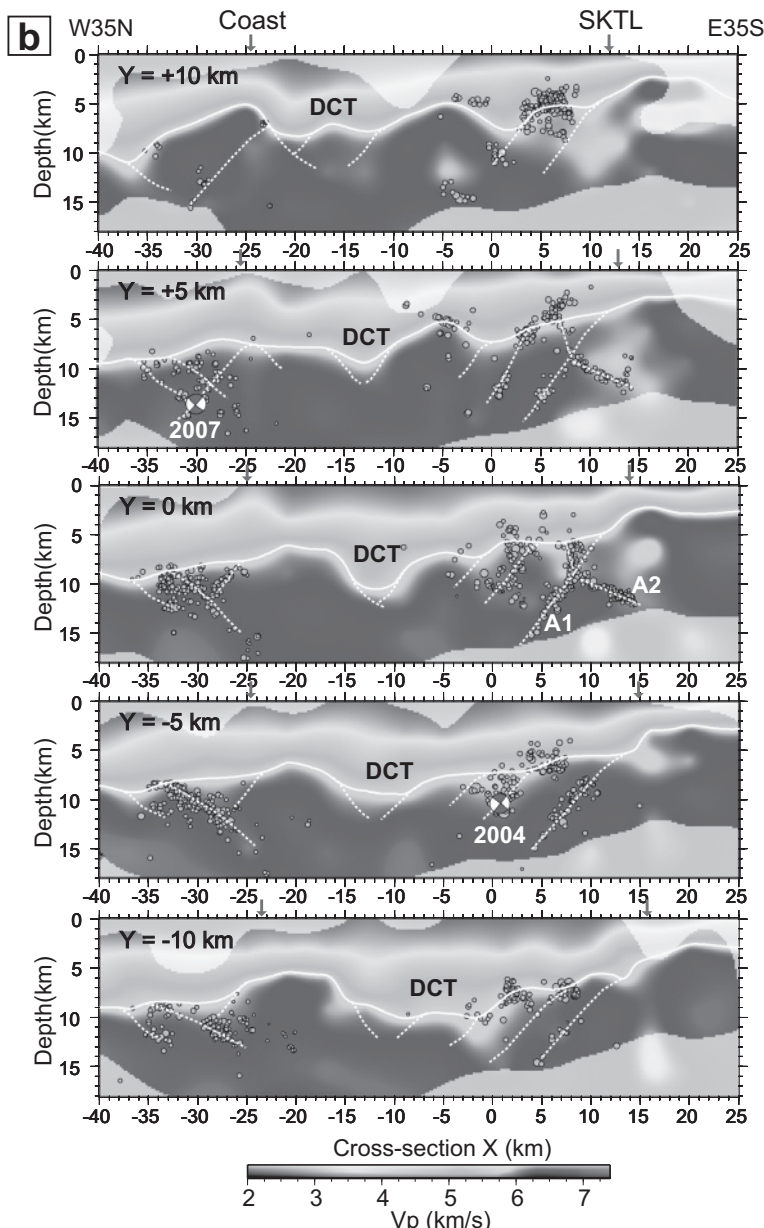


Figure 9.2 (b) Depth sections of the V_p model along W35N-E35S lines in Figure 9.2a. Relocated aftershocks (gray circles) distributed within ± 2.5 km of each line are superimposed. Masked areas correspond to low model resolution. White curves denote iso-velocity contours of $V_p = 5.7$ km/s, and white broken lines show faults suggested from aftershock streaks, top surface geometries of the basement, or velocity changes within the basement. DCT, deep central trough. Blue and red arrows at the top of each section correspond to surface locations of the SKTL and the coastline. Moment tensor solutions for the 2004 and 2007 Niigata earthquakes (NIED) are shown using a lower hemisphere projection rotated into the plane of the section. For color version, see Plates section.

mainshock hypocenter of the 2007 Chuetsu-Oki earthquake appeared to be close to the bottom of a steeply NW-dipping plane. It has been proposed that the mainshock rupture initiated near the bottom of the NW-dipping fault plane and propagated to the southwest and then transferred to the SE-dipping plane across the central crosscutting area of the two faults (Kato *et al.*, 2008a; Takenaka *et al.*, 2009), inferring complex dynamic rupture.

Indeed, Aochi and Kato (2010) modeled the dynamic rupture propagation of the 2007 Chuetsu-Oki earthquake numerically along the inferred segmented fault system using a boundary integral equation method (BIEM). For angles between these fault planes from 80° to 95°, the possibility of rupture transfer from the NW-dipping fault plane to the SE-dipping is numerically demonstrated for any frictional level along fault planes, independently of the crosscutting distance in the center, suggesting two rupture modes. Simultaneous rupture transfer along the overlapping part is possible only under a high-stress load; however, this rupture mode yields an excessively large amount of coseismic slip. Otherwise, where regional stress is relatively low but pore pressure is high enough to cause the rupture (described as the low frictional coefficient case), the rupture transfer to the other fault segment does not occur until rupture terminates on the first fault segment regardless of the crosscutting distance between the two faults. Similarly, the 2009 Suruga Bay intraplate earthquake (M 6.4) in Japan, which occurred within the Philippine Sea plate and had a reverse fault component, showed a similar rupture transfer from one fault segment to the other conjugate segment (Aoi *et al.*, 2010). These recent studies of dynamic rupture process associated with large intraplate earthquakes suggest that rupture transfer or simultaneous ruptures are more common features than previously thought.

9.3.2 Ancient rift system buried beneath thick sedimentary basin

Depth sections of P-wave velocity (V_p) structures show strong lateral heterogeneity (Figure 9.2b), especially orthogonally to the fault strike (Kato *et al.*, 2006a, 2009). Seismic velocities in the hanging wall above the 2004 mainshock fault are lower than those in the footwall at depths shallower than 8 km. We consider that the low-velocity body in the hanging wall corresponds to soft sediments that have accumulated in half-grabens formed by crustal stretching during the opening of the Japan Sea. Conversely, the high-velocity body in the footwall is thought to correspond to the old basement rocks (30 Ma). Here, we define the basement as high-velocity bodies in which V_p is greater than 5.7 km/s (bounded below by the white curves in Figure 9.2b). Most aftershocks seem to be bounded by the basement. The centroid depth of the relocated aftershocks associated with the 2007 mainshock is slightly deeper than that of the 2004 mainshock. This lateral variation of aftershock depths well correlates with that of thickness of sedimentary layers, which on average increases with distance towards the west.

It is important to note that the top surface of the basement on the eastern side ($-5 \text{ km} < X < +15 \text{ km}$) shows clear stepwise structures that gradually deepen in the westward direction. In addition, westward-tilted block structures are interpreted by aftershock streaks, the top

surface geometries of the basement, or velocity changes within the basement (broken white lines in Figure 9.2b). The boundaries between each stepwise and tilted block structure are mainly characterized by west-dipping faults with high dip angles. Near the center of the cross-sections ($X \sim -10$ km), the top surface of the basement reaches its deepest depth (~ 10 km thickness of sediments) and then rises sharply to the coastline ($X = -25$ km). This concave basement structure forms a deep central trough (DCT) filled with thick sediments between the source areas of the two Niigata earthquakes. In contrast, on the western side of the DCT ($X < -20$ km), the stepwise block structures are primarily tilted eastward with low dip angles (eastward-dipping low-velocity zones located just above the 2007 aftershock alignments along $Y = -5$ and -10 km), although westward-tilted structures also developed, especially in the north sections ($Y > +5$ km) showing complete inversion; in short, the west block appears to hang over the footwall. The stepwise and tilted block structures are observed along all of the cross-sections (Figure 9.2b), with block widths ranging from 5 to 10 km.

Furthermore, a very fine scale (~ 1 km grid) seismic tomography using a linear seismic array in the southwestern edge of the source region in the 2004 Chuetsu earthquake confirmed that the aftershocks appear to be aligned along pre-existing boundaries of the step-like array of tilted block structures (Kato *et al.*, 2010b; Figure 9.3). With deepening of the basement-cover contact to the west, the sedimentary succession in the hanging wall deepens to about 9 km. Indeed, the westward-tilt of the sedimentary strata was delineated by a seismic reflection survey conducted by the Japan National Oil Corporation (JNOC, 1988) in the vicinity of the studied area (Sato and Kato, 2005). The velocity model within the sedimentary basin correlates well with the seismic reflection profile. The surface elevation increases towards the southern part of the SKTL (Muikamachi fault), which illustrates that the cover sequence has been deformed by upward movements of the step-like tilted blocks in the basement. There seem to be three plateaus within the topography to the west of the Muikamachi fault trace (gray horizontal lines in the top graph in Figure 9.3). We therefore hypothesize that these plateaus might be created by both upward movements of the three tilted blocks and compressive deformations of the sedimentary strata in the hanging wall through compressional inversion.

The stepwise and tilted block structures as described above are clear evidence of the buried Miocene rift system formed during the spreading of the Japan Sea. It is worthwhile noting that the aftershock distributions associated with the two Niigata earthquakes correlated well with these complex and heterogeneous structures. Most aftershocks are aligned along the NW-dipping faults with high dip angles ($\sim 60^\circ$) or along the SE-dipping faults with low-dip angles ($\sim 35^\circ$) (Kato *et al.*, 2006a; Shinohara *et al.*, 2008). These fault planes are orthogonal to each other, and correspond roughly to the boundaries of the tilted blocks. These results suggest that the seismogenesis of the two Niigata earthquakes was due primarily to compressional inversion tectonics involving pre-existing structures related to the Miocene rift system. Since pre-existing faults within the ancient rift system are weak due to thermal softening (Hansen and Nielsen, 2003) and over-pressurized fluids beneath the seismogenic zone (Sibson, 2007), these faults are mechanically easy to reactivate as

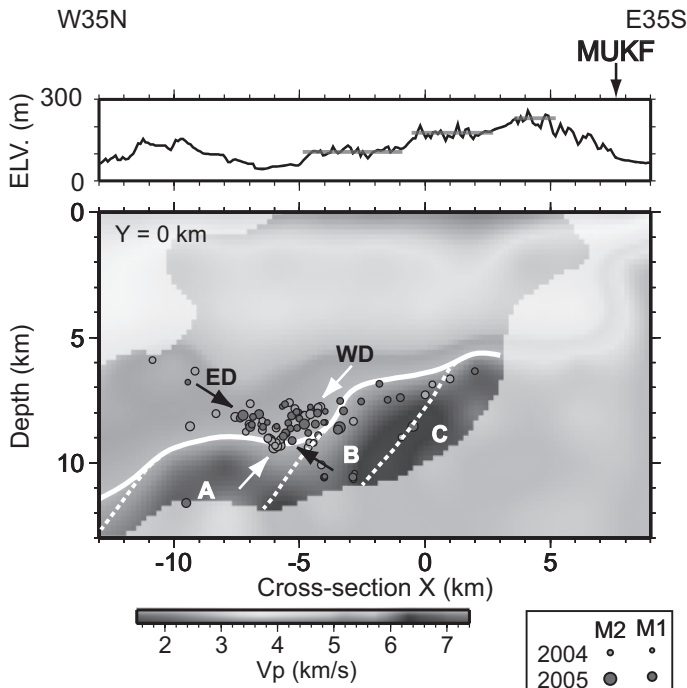


Figure 9.3 Depth section through the V_p model obtained at the southwest edge of the source area of the 2004 Chuetsu earthquake, with superimposed relocated aftershocks distributed within ± 4 km from the section (light gray circles observed in 2004, and dark gray circles in 2005) (Kato *et al.*, 2010b). Masked areas correspond to low model resolution. White curves denote iso-velocity contours of $V_p = 5.7$ km/s, and white broken lines show faults suggested from aftershock alignments and the top surface geometries of the basement. Three tilted blocks are labeled as A, B, and C. Eastward- and westward-dipping alignments of aftershocks near the top surface of the basement are indicated by black (ED) and white (WD) arrows. The top figure shows a topography variation along the profile. Gray lines correspond to the three plateaus in the topography. MUKF is the surface trace of the Mui-kamachi fault.

reverse faults under compression. Indeed, the NW-dipping fault planes with high dip angles are far from an optimal orientation against the regional stress field (e.g., Kato *et al.*, 2006a; Townend and Zoback, 2006; Terakawa and Matsu'ura, 2010), which means that those NW-dipping faults are mechanically weak.

The planar distribution of V_p at a depth of 9 km (Figure 9.4a) shows that the DCT between the two source areas extends continuously for over 20 km from south to north. The azimuth of the DCT filled with thick sediments lies almost parallel to the surface traces of major active faults and fold axes. In contrast, remarkable high-velocity bodies ($V_p = \sim 6.8\text{--}7.1$ km/s) are imaged beneath the DCT ($-15 \text{ km} < X < -5 \text{ km}$) and the source region of the 2007 earthquake (deeper than 15 km, in Figures 9.2b and 9.4b). As a result, the velocity gradient of V_p with depth is very steep at the DCT. We consider that the DCT corresponds to the Miocene rift axis, because the dominant dip direction of each tilted

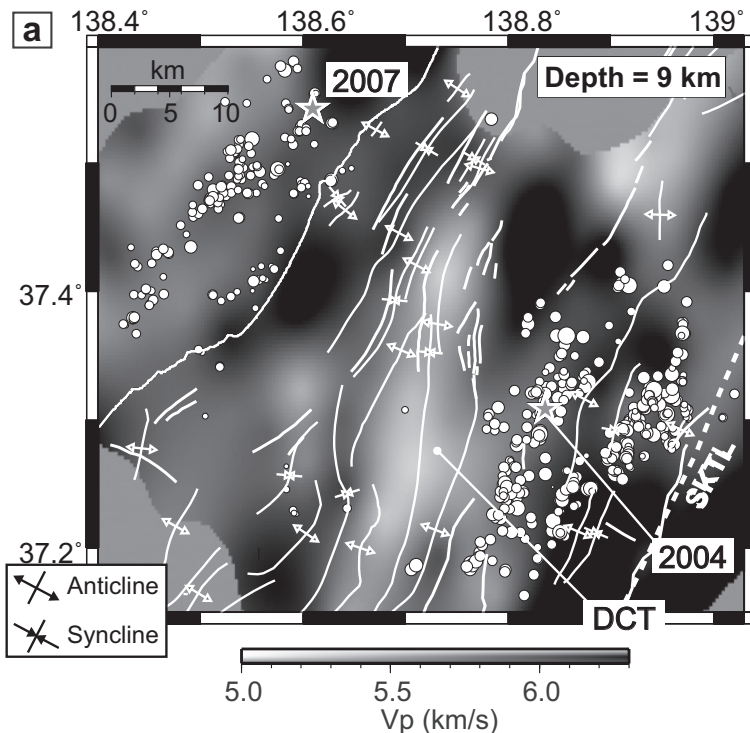


Figure 9.4 Map views of V_p structures at representative depths (Kato *et al.*, 2009). (a) 9 km. Relocated aftershocks distributed at depths from 7.5 km to 10.5 km (white circles) are superimposed. Gray stars denote epicenters of the 2004 and 2007 mainshocks. Major active faults are drawn as white lines. Anticlines and synclines are represented by white lines with arrows. A broken line indicates the SKTL.

block changes from westward to eastward across it. Based on laboratory measurements of exposed rocks (Christensen, 1996), we interpret the high-velocity bodies beneath the DCT to be a diabase intrusion into the Miocene rift axis. We propose that the diabase body intruded into the upper crust, acting as a magma source within the extensional rift system during the opening of the Japan Sea (Bjorklund *et al.*, 2002; White *et al.*, 2008; Figure 9.5). Indeed, andesitic and basaltic rocks are partially exposed on the surface in the study area (GSJ, 2002).

The spatial correlation of the DCT with the surface traces of major active faults and fold axes (Figure 9.4a) illustrates that the major active faults have slipped in response to upward movements of the stepwise and tilted blocks in the basement, which moved as a result of the horizontal compressional stress (Figure 9.5). These upward movements have led to the active growth of anticlinal folds. The elevations of topographic hills on the eastern side of the DCT are higher than those on the western side, due to a difference in dip angles of faults in the basement crossing the Miocene rift axis. Additionally, it is worth noting

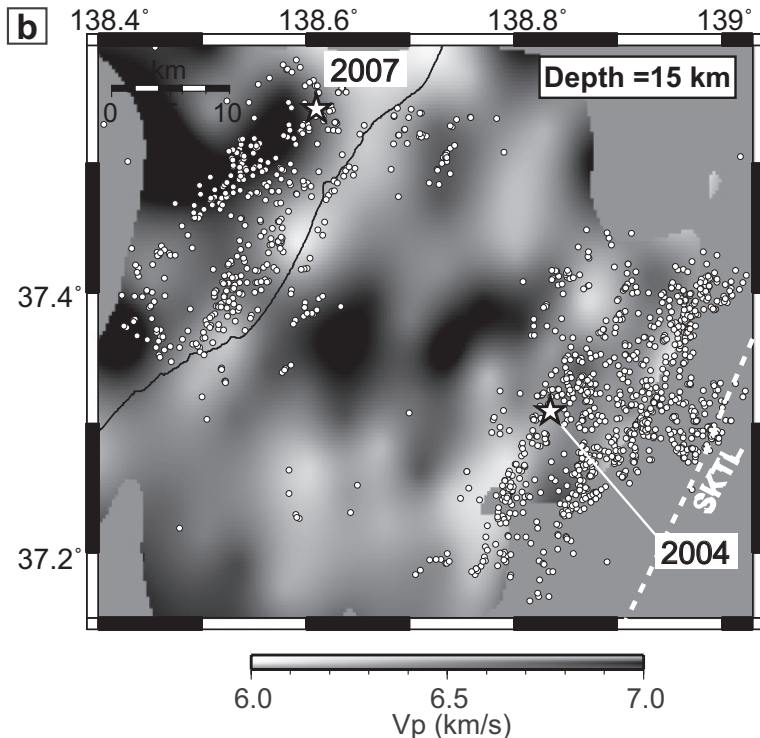


Figure 9.4 (b) 15 km. The center of the gray scale corresponds to an average velocity calculated at this depth (6.5 km/s). All of the relocated aftershocks (white circles) are superimposed.

that the eastward- or westward-dipping faults on the flanks of the DCT are situated along mechanically weak structural boundaries between the thick sediment and the basement (Figure 9.5).

The geometries of the block structures associated with the ancient rift system change along the fault strike in the vicinity of the cross-section at around $Y = 0$ km in Figure 9.2b. In the source region of the 2004 Chuetsu earthquake, the thickness of sedimentary layers in the hanging wall increases markedly on the southwest side of the mainshock hypocenter (e.g., Kato *et al.*, 2006a). For the case of the 2007 Chuetsu-Oki earthquake, a southeast-tilted basement structure dominates in the south, whereas a northwest-tilted basement structure gradually develops towards the north (e.g., Kato *et al.*, 2008a). These spatial variations indicate the presence of a segment boundary of the block structure near the cross-section of $Y = 0$ km in Figure 9.2b.

9.3.3 Stress loading processes to the reactivation of the ancient rift system

Even if several ancient weak fault zones in the upper crust exist within the buried rift system, a driving force to reactivate them is needed. We here discuss the mechanisms of stress loading into source faults of intraplate earthquakes in the Niigata region.

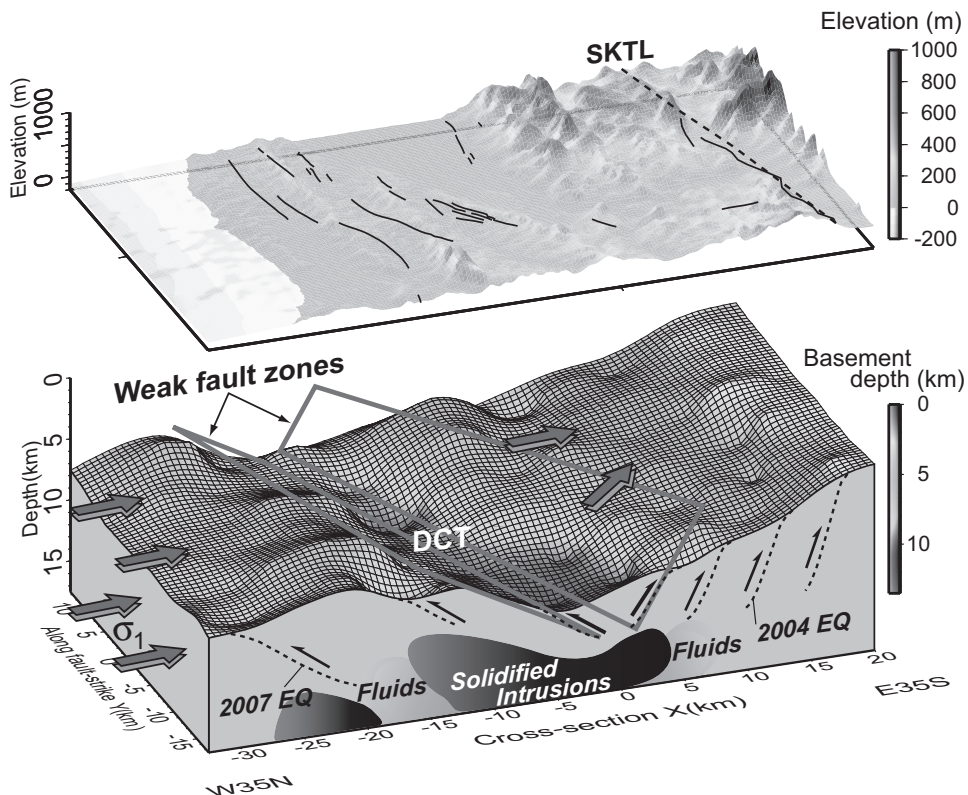


Figure 9.5 Three-dimensional perspective views of active tectonics in the study area (modified after Kato *et al.*, 2009). (Top) Topography, over which active faults are drawn as solid lines. The broken line indicates the SKTL. (Bottom) Perspective image of the depth to $V_p = 5.7$ km/s with interpretations. Gray rectangles denote potential weak fault zones along the flanks of the DCT. Dominant reactivated normal faults are drawn as broken lines with arrows showing slip directions during compressional inversion. Large arrows indicate the inferred direction of the maximum stress σ_1 . Note that the σ_1 axis rotates from W30°N–E30°S in the central area of the source region of the 2004 Chuetsu earthquake to the E–W horizontal direction in the southwestern area. For color version, see Plates section.

The spatial variation of stress fields in the source area of the 2004 Chuetsu earthquake provides us with a valuable opportunity to understand the deformation of sedimentary layers in the hanging wall (Kato *et al.*, 2006a). Results of stress tensor inversions using dense aftershock data (focal mechanisms) show that the maximum principal stress rotates from W30°N–30°S in the central area of the source region to the E–W horizontal directions in the southwestern area (Figure 9.5). In short, the compressional stress axis in the southwest area is oblique to the fault strike of N35°E, even though the compressional stress axis in the central part is almost perpendicular to the fault strike. Near the hypocenter of the mainshock rupture, the thickness of sediment layers in the hanging wall increases towards E35°S, as well as increasing in the S35°W direction. As a result, the iso-velocity contour of

$V_p = 5.7$ km/s undergoes a marked change around the mainshock hypocenter (Figure 9.5). The structural coincidence between the stress axis distribution and the velocity structure raises the possibility that rotation of the compressional stress axis in the southwest area might be caused by lateral variation of sediment layers in the hanging wall. Sediments in the hanging wall with low elastic modulus can potentially allow ductile flow along the fault zone when compressional shear stress is applied. The ductile deformation of the sediments can partially accumulate elastic strain in the brittle parts of the fault zone, and may play a role in stress loading. Although it is difficult to directly demonstrate the stress loading process by the ductile deformation of the sediments into source faults, there is geodetic evidence showing ongoing ductile deformation of the sediments. For example, following the 2007 Chuetsu-Oki earthquake, episodic growth of fault-related folds in the shallow sedimentary layer was clearly detected by SAR interferometry, and did not accompany any seismicity (Nishimura *et al.*, 2008). The long-term leveling measurement also supports the episodic growth of folds therein.

In addition to the deformation of sediments, it has been proposed that ductile creeping of the weak lower crust could cause stress loading into seismogenic faults (Iio *et al.*, 2002). Note that slow anomalies in the lower crust ($V_p = \sim 6.1\text{--}6.3$ km/s) are localized around deep extensions of mainshock faults for the 2004 and 2007 Niigata earthquakes (Figures 9.4b and 9.5). Furthermore, a highly conductive body was found in the lower crust (deeper than 15 km) beneath the source region of the 2004 earthquake by wideband magnetotelluric survey (Uyeshima *et al.*, 2005). Thus, these slow anomalies in the lower crust probably represent crustal fluids that might be exsolved from the solidified intrusions beneath the rift axis. According to a regional (larger-scale) tomography study conducted in the Niigata region (Nakajima and Hasegawa, 2008), these slow anomalies appear to extend to the deeper part of the crust and connect to a distinct low-velocity zone beneath the Moho ($\sim 30\text{--}50$ km depth) under source areas of the two Niigata earthquakes. Similarly, from the backbone mountain range to the fore-arc side of northeast Japan, several low-velocity zones are recognized just below the source areas of large intraplate earthquakes (e.g., Okada *et al.*, 2010). In the cases of the 2003 North Miyagi earthquake and the 2008 Iwate-Miyagi Nairiku earthquake, the upper crustal structures implying an ancient rift system were imaged by temporary dense seismic observations conducted after those mainshocks, as well as the low-velocity zones below the source areas (Okada *et al.*, 2007, 2012). Several seismic reflection profiles also confirmed that reverse-fault reactivation of pre-existing Miocene normal faults occurred across the entire seismogenic zone in the fore-arc side of northeast Japan (Kato *et al.*, 2006b).

Since the strength of ductile creep, which is a dominant deformation process in the lower crust, is weakened by crustal fluids (e.g., Carter and Tsenn, 1987), the slow anomalies in the lower crust correspond to locally weak zones (Iio *et al.*, 2002). Concerning the deformation process in the weak zone, Iio *et al.* (2002) assumed that the weak zone consists of numerous aseismic faults since the deformation is thought to be localized in ductile shear zones. Thus, local ductile creep of the weak zone within the lower crust causes stress loading, or stress transfer to the upper ancient rift system (Kenner and Segall, 2000), leading to the reactivation

of this system in the form of intraplate earthquakes. Since the width and depth of the weak zones provide constraints on the process of stress loading to intraplate earthquakes, detailed knowledge of the heterogeneity within the lower crust is quite important.

9.3.4 Numerical modeling of development of fault zones

Using finite element modeling incorporating visco-elasto-plasticity, Shibasaki and Kato (2012) numerically simulated the development of fault zones in a geological setting with thick sedimentary layers and weak zones in the basement inferred from the tomographic study in the Niigata region (Figure 9.2b; Kato *et al.*, 2009). It is assumed that values of elastic constants and frictional coefficients in the sedimentary layer are smaller than those in the basement. Furthermore, they assumed that the frictional coefficient in the basement is low in areas of low P-wave velocity, examining how the present rheological structures inferred from P-wave velocity structure affect the development of fault zones. Figure 9.6 shows the equivalent total strains defined for the deviatoric components of the total strains after 8.0×10^4 years (i.e., the amount of contraction is 1.2 km). The equivalent total strains include viscous, plastic, and elastic strains. Fault zones are created just above concavities along the boundary between the lower sedimentary layer and the basement. For example, along all sections, fault zones are well developed at locations where the effective frictional coefficient is low in the basement and above the DCT, confirming the development of a NW-dipping reverse fault zone, which was activated by the mainshock of the 2004 Chuetsu earthquake. The model also shows the development of NW-dipping faults that were parallel to the fault of the mainshock. These faults may correspond to the faults of large aftershocks follow the 2004 Chuetsu earthquake. In addition, the model shows the development of SE-dipping reverse fault zones that were activated by the mainshock of the 2007 Chuetsu-Oki earthquake. Thus, the numerical results indicate that buried rift and weak zones in the basement caused the development of the complex fault configuration observed in the Niigata region.

9.4 The 2007 Noto-Hanto earthquakes

A shallow M_{JMA} 6.9 inland earthquake occurred on the west coast of the Noto Peninsula in Japan on March 25, 2007. The focal mechanism estimated by moment tensor inversion (NIED) revealed a dominant reverse slip component with a strike of approximately N55°E (Figure 9.7a). The Noto Peninsula is situated close to the Yamato Basin in the Japan Sea, which is a large rift basin formed during the extension stage of the Japan Sea (e.g., Shimazu *et al.*, 1990). Based on geological studies of early Miocene syn-rifting succession in the northern regions of the Noto Peninsula (e.g., Kano *et al.*, 2002), it is proposed that small-scale rift structures were formed along the northern coast of the Noto Peninsula during the extension stage of the Japan Sea. Following the 2007 Noto-Hanto earthquake, we deployed a total of 89 temporary seismic stations on land in the source region. The seismic network was densely deployed with station spacing averaged less than 2 km (Figure 9.7a).

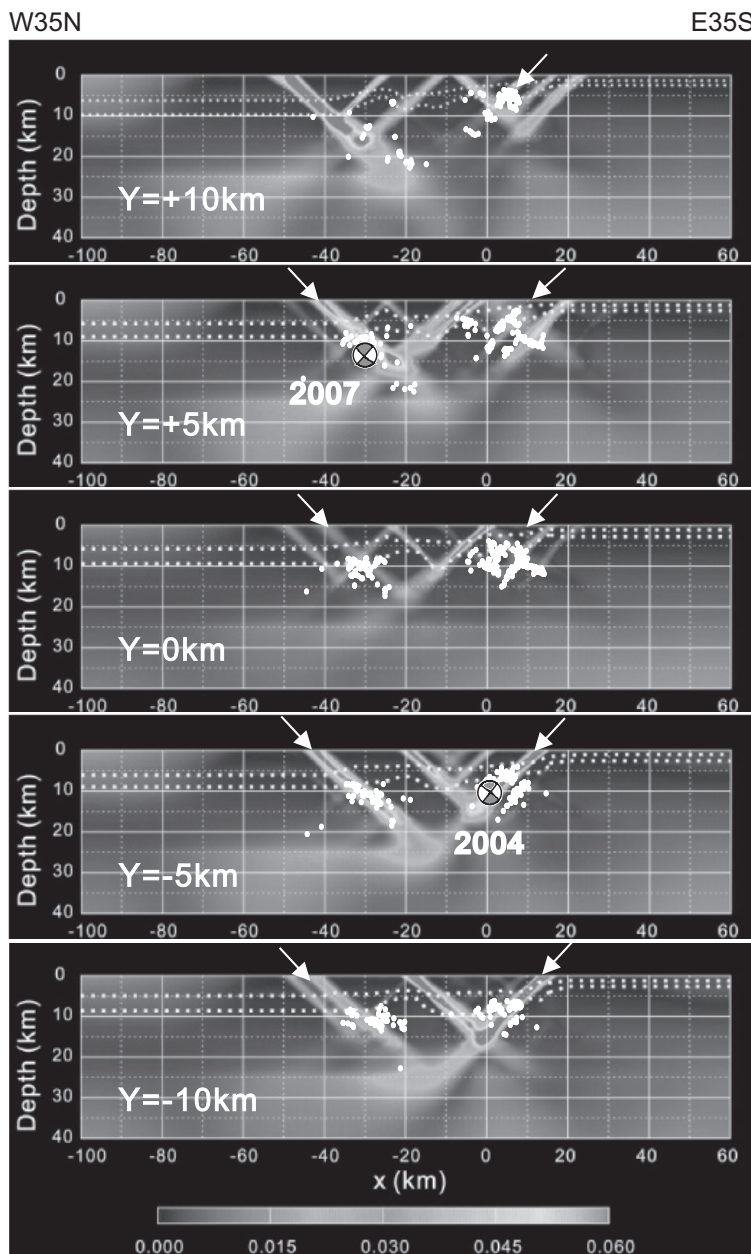


Figure 9.6 Numerical modeling of equivalent total strain in each cross-section shown in Figure 9.2b (Shibazaki and Kato, 2012). Viscous, plastic, and elastic strains are included in the total strain. Strain weakening in plastic deformation is incorporated. White arrows indicate the fault zones corresponding to the 2007 Chuetsu-Oki (left) and 2004 mid-Niigata Prefecture (right) earthquakes. The upper and lower dotted lines indicate the boundaries between the upper and lower sedimentary layers and between the lower sedimentary layer and the basement. White circles indicate the locations of aftershocks from the 2004 and 2007 earthquakes, as determined by Kato *et al.* (2009).

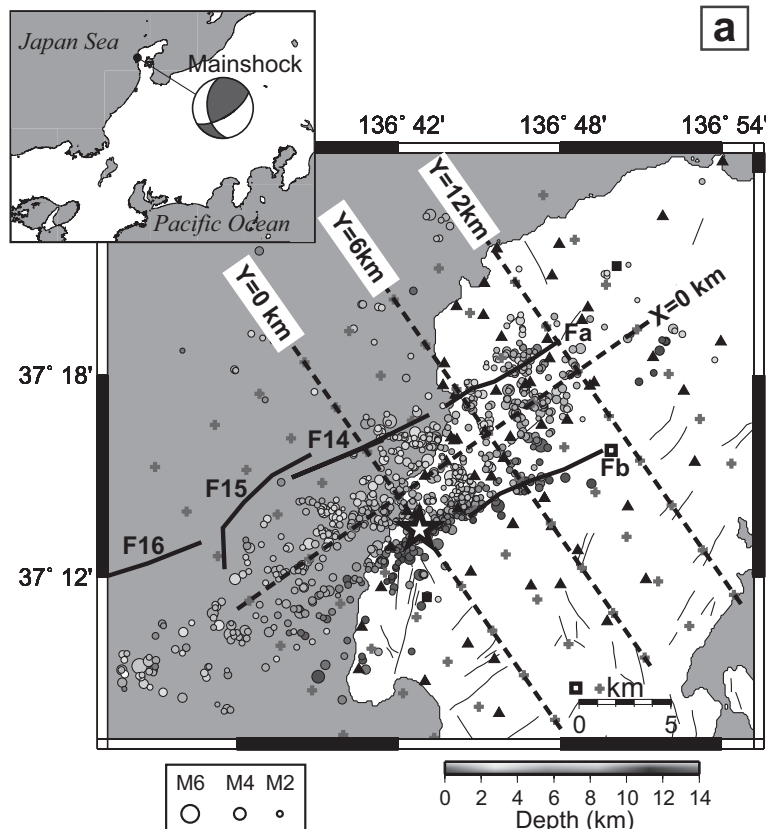


Figure 9.7 Dense seismic observations and V_p model in the source area of the 2007 Noto-Hanto earthquake (modified after Kato *et al.*, 2008b). (a) Map of the relocated aftershock hypocenters with the circle size scaled to earthquake magnitude and tones scaled to depth. The star denotes the epicenter of mainshock. The inset indicates the location of the area investigated with moment tensor for the mainshock (NIED). Filled triangles and squares denote temporary seismic stations and online stations, respectively. Open squares are temporary online stations operated by the Japanese University Group of the Joint Seismic Observations at NKTZ (2005). The grid used in the tomography is shown by crosses. Active (F14–F16) and geological faults (Fa, Fb) associated with the present earthquake are drawn as thick solid lines, and the other major active faults are drawn as thin solid lines.

9.4.1 Aftershock distribution and pre-existing structures within ancient rift system

Figure 9.7b shows the P-wave velocity (V_p) along five cross-sections perpendicular to the fault strike along relocated aftershocks within ± 1.5 km of the section. Based on the aftershock distributions, it is estimated that the mainshock occurred on the approximately 55° southeastward-dipping plane. Surface extension of the mainshock fault roughly corresponds to the surface traces of several active faults beneath the ocean (F14–F16) and a

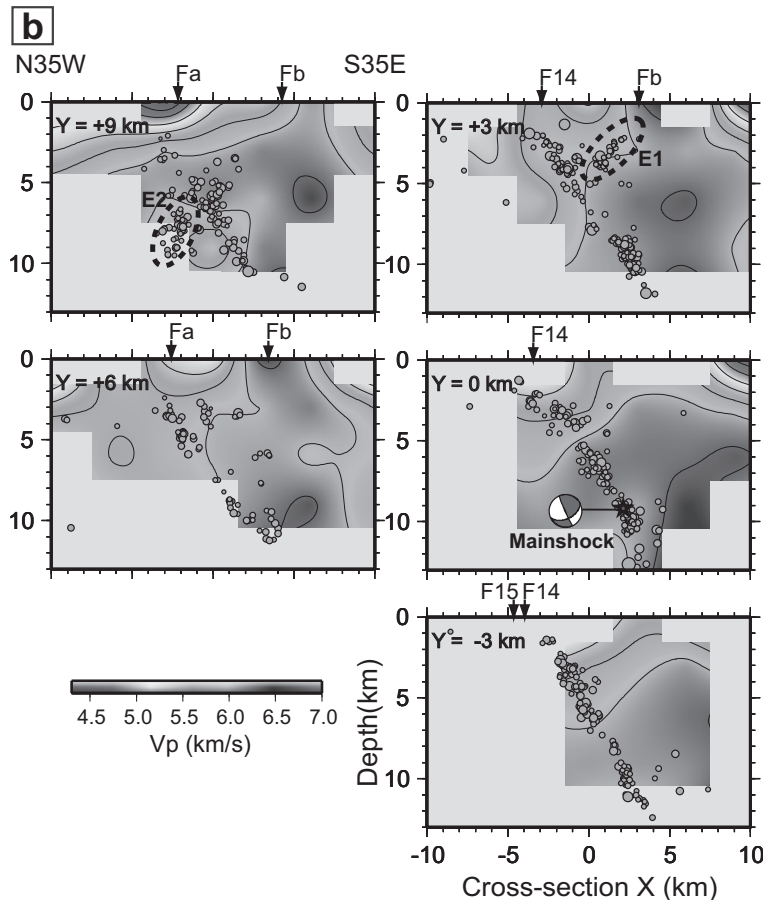


Figure 9.7 (b) Depth sections through the V_p model with superimposed relocated aftershocks distributed within ± 1.5 km of each cross-section. The white-masked areas correspond to the low-resolution model. The contour line interval is 0.3 km/s. Dashed ellipses (E1, E2) are explained in text. Arrows at the top of each section denote the approximate surface locations of faults.

geological fault (defined as a fault for which activity history has not been recognized since the Quaternary period) F_a (Katagawa *et al.*, 2005).

P-wave velocities of the hanging wall in the southeast appear to be higher than those of the footwall in the northwest. In addition, the high- V_p body of the hanging wall has a slightly high V_p/V_s ratio ($\sim 1.75\text{--}1.8$), while the low- V_p body in the footwall appears to have a low V_p/V_s ratio ($\sim 1.6\text{--}1.7$) at depths greater than 3 km in the cross-sections (see Figure 2 in Kato *et al.*, 2008b). The aftershocks associated with the mainshock fault are distributed approximately along this SE-dipping velocity boundary. Based on these observations, we propose that the rupture of the Noto-Hanto earthquake was likely to have propagated along these pre-existing faults. In addition to the mainshock faults, NW-dipping alignment of

aftershocks with an angle of 50° is approximately distributed on a velocity boundary at shallow and moderate depths (E1 and E2 in Figure 9.7b). The surface extension of this NW-dipping velocity boundary almost coincides with geological fault F_b (Figure 9.7a).

Near-surface thin layers with significantly low V_p (<5.0 km/s) and high V_p/V_s (>1.9) were imaged to the northwest of the mainshock epicenter ($X < \sim 0$ km). This slow layer corresponds to the sediments that have piled over the half-grabens formed by crustal stretching at the time of expansion of the Japan Sea. Since the thickness of the sediments is less than approximately 3 km, the extent of the crustal stretching is considered to be less significant compared with the Niigata region (Figure 9.2b).

Geological studies show that the crustal shortening that began in the late Miocene (e.g., Itoh and Nagasaki, 1996) has continued to the present and led to the reactivation of a fault that formed as a normal fault under an extensional stress field. The SE-dipping fault plane of the mainshock with high dip angle for a thrust-type event is unfavorably oriented in the direction of the regional maximum stress, which is almost horizontally compressional to the WNW–ESE strike (e.g., Terakawa and Matsu’ura, 2010). This implies that the mainshock fault plane is mechanically weak. Therefore, a likely explanation for the Noto-Hanto earthquake involves reactivation of a normal fault as a reverse fault in terms of inversion tectonics. The tomographic images associated with the inverted normal fault were also observed in the source region of the 2004 and 2007 Niigata earthquakes, as mentioned in the previous sections.

9.4.2 Crustal fluid beneath the mainshock hypocenter

Interestingly, the dip angle of the aftershock alignment changes markedly from 55° to nearly 90° beneath the mainshock hypocenter in the cross-section of $Y = 0$ km (Figure 9.7b). In addition, the epicenter distributions of these aftershocks beneath the mainshock hypocenter were linearly concentrated along the fault strike of N55°E (Figure 9.7a) and the size of the vertical aftershock alignment was approximately 3 km × 3 km. Interestingly, both the mainshock hypocenter and the vertical alignment of aftershocks beneath it are located in the relatively low- V_p zones where the low- V_p/V_s values were imaged. According to Takei (2002), the relatively low V_p/V_s and low V_p can be explained by the presence of water-filled pores with high aspect ratios. The study of the stress field using high-quality aftershock data showed that aftershocks that occurred above 4 km in depth indicated a strike-slip stress regime (Kato *et al.*, 2011; Figure 9.8). In contrast, aftershocks in deeper parts (>7 km) indicated a thrust-faulting stress regime. In addition to this depth variation of the stress field, the maximum principal stress (σ_1) axis was stably oriented approximately W20°N down to the depth of the mainshock hypocenter, largely in agreement with the regional stress field, but below that depth the σ_1 axis had no definite orientation, indicating horizontally isotropic stress. One likely cause of these drastic changes in the stress regime with depth is the buoyant force of a fluid reservoir localized beneath the seismogenic zone. Indeed, the detection of a conductive layer beneath the mainshock hypocenter by a magnetotelluric

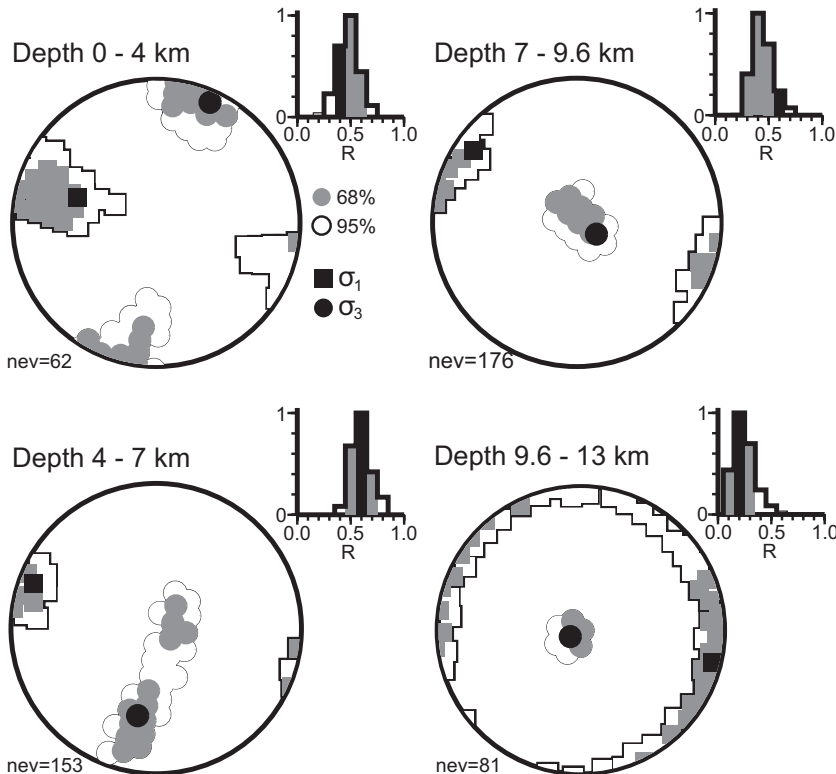


Figure 9.8 Results of stress tensor inversion for four depth ranges (Kato *et al.*, 2011): 0–4 km, 4–7 km, 7–9.6 km, and 9.6–13 km, showing lower-hemisphere equal-area projections of the orientations of σ_1 (squares) and σ_3 (circles), each with their marginal confidence limits. Black-filled symbols, optimal solutions. Gray shades, 68% confidence limits. Open contours, 95% confidence limits. In the top right margins, frequency histograms of the R-values, with 68% and 95% confidence intervals denoted by gray and open bars, respectively. In the bottom left margins, the number of events is shown.

survey (MT) conducted after the occurrence of the mainshock (Yoshimura *et al.*, 2008) supports the interpretation of the presence of water (Figure 9.9).

Given that σ_1 corresponds to the maximum horizontal stress (σ_h^{\max}), the transition of the stress field with depth may be explained by an increase in magnitude of the minimum horizontal stress (σ_h^{\min}). One simple candidate for the origin of such an increase is a hypothetical, upward flexure of the upper crust, with its hinge axis oriented parallel to the σ_1 axis (Figure 9.9). In shallow parts, σ_h^{\min} remains smaller than σ_v (vertical stress) because of extensional stresses associated with the bending ($\sigma_v = \sigma_2$, $\sigma_h^{\min} = \sigma_3$), resulting in a strike-slip regime. In deeper parts, by contrast, σ_h^{\min} becomes larger than σ_v because of compressional stresses associated with the bending ($\sigma_h^{\min} = \sigma_2$, $\sigma_v = \sigma_3$), which leads to a thrust-faulting regime. At great depths, σ_h^{\min} ($= \sigma_2$) grows very close to σ_h^{\max}

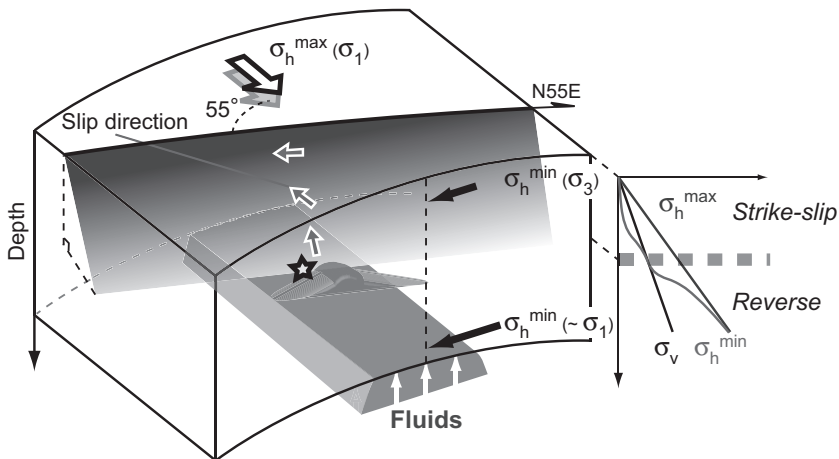


Figure 9.9 Schematic image of the depth variations in the stress field and a hypothetical fluid reservoir beneath the 2007 Noto-Hanto mainshock hypocenter (star) (Kato *et al.*, 2011). The lengths of vectors are scaled to the magnitudes of the principal stresses that they represent. The fault plane is shown as a shaded, inclined surface. Gray arrows, slip directions derived from a finite source model (Ozawa *et al.*, 2008).

($= \sigma_1$), resulting in a horizontally isotropic stress field. A possible support for this hypothesis comes from geomorphological data, where the height profile of a marine terrace formed about 120,000 years ago (Ozawa *et al.*, 2008) hints at the presence of a similar upward flexure in the earthquake source region.

We hypothesize that the buoyant force of a fluid reservoir beneath the mainshock hypocenter is causing such an upward flexure of the upper crust. Our study has only indicated localization of fluids just beneath the mainshock hypocenter, but regional (larger-scale) tomography (Hasegawa *et al.*, 2009) has suggested that fluids are apparently infiltrating into the seismogenic zone from a deeper and larger fluid reservoir, located at approximately 20 km in depth.

It has been postulated that fluids are involved in the initiation of mainshock ruptures (e.g., Miller *et al.*, 2004). According to the fault-valve model (e.g., Sibson, 2007), for example, high-pressured fluids intrude episodically into the fault region, reduce shear strengths, and induce mainshock ruptures. In fact, weak phases in the 2007 Noto-Hanto earthquake waveforms, observed at several seismic stations, have revealed the occurrence of an initial breakdown rupture close to the mainshock hypocenter (Sakai *et al.*, 2008). Furthermore, several foreshocks were identified in the vicinity of the mainshock hypocenter approximately 10 minutes prior to the rupture initiation. These observations lead us to propose the following scenario for the rupture propagation. The initiated rupture is likely to have propagated along the structural boundary between the hanging wall and the footwall, though it was oriented unfavorably for failure. It is likely that fluid migrations, which triggered the initial breakdown, continued to proceed into broader areas along the structural

boundary, reducing shear strengths and facilitating ruptures there. Given these considerations, we hypothesize that fluid migrations along the fault, along with relative mechanical weaknesses within the fault zone, were the principal factors that caused the 2007 Noto-Hanto earthquake by reactivating a pre-existing normal fault created during the opening of the Japan Sea.

9.5 Conclusions

We imaged the entire crustal structure and stress field of buried ancient rift systems including heterogeneity within the crust through the seismic-tomographic analysis utilizing a dense seismic network deployed immediately after three recent large intraplate earthquakes along the eastern margin of the Japan Sea. We discovered that stepwise and tilted block structures of the basement, which are geophysical evidence of a Miocene rift system, are widely distributed beneath the thick sedimentary basin in the Niigata region. A similar structure associated with the ancient rift system was imaged in the source area of the Noto-Hanto earthquake. Mainshock fault planes with high dip angles are far from an optimal orientation against the regional stress field, which means that those faults are mechanically weak. Most aftershocks following recent intraplate earthquakes align roughly along the tilted block boundaries of the basement and are controlled by weaknesses associated with buried rift systems.

Furthermore, the structural coincidence between the stress axis distribution and the velocity structure observed in the Niigata region raises the possibility that ductile deformation of the sediments can partially accumulate elastic strain in the brittle parts of the fault zone. In addition, low-velocity anomalies are localized beneath the seismogenic zones, indicating that fluids may have locally weakened the crust. This study therefore suggests that reactivation of pre-existing faults within ancient rift systems by stress loading through ductile flow in the upper crust and creeping of the locally weakened lower crust is a plausible mechanical explanation for intraplate earthquakes. We believe that this mechanical explanation is applicable to other intraplate earthquakes in compressional inverted basins, beneath which ancient rift systems may exist, such as the New Madrid seismic zone (NMSZ) (Kenner and Segall, 2000), and the El Asnam fault zone in Algeria (Chiarabba *et al.*, 1997). In the NMSZ, a local low-velocity anomaly in the lower crust and upper mantle is imaged along the seismically active zone (Zhang *et al.*, 2009). These weak zones may transfer stress to the upper crust when loaded, thus leading to repeated shallow earthquakes in the NMSZ, which is a similar picture to that illuminated along the eastern margin of the Japan Sea.

In order to deepen our understanding of intraplate earthquake generation, a more quantitative approach such as numerical simulation is quite important. Although Shibasaki and Kato (2012) explored the possibility of clarifying the relationship between the configuration of fault zones and the heterogeneous crustal structure deduced from seismic tomography, more information is required on the distribution of pre-existing weak fault zones in order

to perform more realistic modeling of fault development. Therefore, we need to implement numerical models by developing rheological models within and beneath seismogenic zones (crust and mantle) through a multi-disciplinary study consisting of dense seismic and electromagnetic surveys, geological observations, and laboratory measurements.

References

- Aochi, H., and Kato, A. (2010). Dynamic rupture of crosscutting faults: a possible rupture process for the 2007 M_w 6.6 Niigata-ken Chuetsu-Oki earthquake. *Journal of Geophysical Research*, 115, B05310, doi:10.1029/2009JB006556.
- Aoi, S., Enescu, B., Suzuki, W., et al. (2010). Stress transfer in the Tokai subduction zone from the 2009 Suruga Bay earthquake in Japan. *Nature Geoscience*, 3, 496–500, doi:10.1038/ngeo885.
- Bjorklund, T., Burke, K., Zhou, H., and Yeats, R. S. (2002). Miocene rifting in the Los Angeles Basin: evidence from the Puente Hills half-graben, volcanic rocks, and P-wave tomography. *Geology*, 30, 451–454.
- Carter, N. L., and Tsenn, M. C. (1987). Flow properties of the continental lithosphere. *Tectonophysics*, 136, 27–63.
- Chiarabba, C., Amato, A., and Meghraoui, M. (1997). Tomographic images of the El Asnam fault zone and the evolution of a seismogenic thrust-related fold. *Journal of Geophysical Research*, 102, 24485–24498.
- Chiarabba, C., De Gori, P., and Boschi, E. (2009). Pore-pressure migration along a normal-fault system resolved by time-repeated seismic tomography. *Geology*, 37, 67–70. doi:10.1130/G25220A.1.
- Christensen, N. I. (1996). Poisson's ratio and crustal seismology. *Journal of Geophysical Research*, 101, 3139–3156.
- Geological Survey of Japan, AIST (2002). *Geological Map of Japan*, CD-ROM Version, Digital Geoscience Map G-3.
- Hansen, D. L., and Nielsen, S. B. (2003). Why rifts invert in compression. *Tectonophysics*, 373, 5–24.
- Hasegawa, A., Nakajima, J., Uchida, N., et al. (2009). Plate subduction, and generation of earthquakes and magmas in Japan as inferred from seismic observations: an overview. *Gondwana Research*, 16, 370–400, doi:10.1016/j.gr.2009.03.007.
- Iio, Y., Sagiya, T., Kobayashi, Y., and Shiozaki, I. (2002). Water-weakened lower crust and its role in the concentrated deformation in the Japanese Islands. *Earth and Planetary Science Letters*, 203, 245–253.
- Iio, Y., Sagiya, T., and Kobayashi, Y. (2004). Origin of the concentrated deformation zone in the Japanese Islands and stress accumulation process of intraplate earthquakes. *Earth, Planets and Space*, 56, 831–842.
- Itoh, Y., and Nagasaki, Y. (1996). Crustal shortening of southwest Japan in the late Miocene. *The Island Arc*, 5, 337–353, 1996.
- JNOC (1988). *Report on basic geophysical exploration in onshore area “Kubiki-Tamugiyama”*. Tokyo: Japan National Oil Corporation (in Japanese).
- Kano, K., Yoshikawa, T., Yanagisawa, Y., Ogasawara, K., and Danhara, T. (2002). An unconformity in the early Miocene syn-rifting succession, northern Noto Peninsula, Japan: evidence for short-term uplifting precedent to the rapid opening of the Japan Sea. *The Island Arc*, 11, 170–184.

- Katagawa, H., Hamada, M., Yoshida, S., *et al.* (2005). Geological development of the west sea area of the Noto Peninsula district in the Neogene Tertiary to Quaternary, central Japan. *Journal of Geography*, 114, 791–810.
- Kato, A., and the research team of aftershock observations for the 2004 mid-Niigata Prefecture Earthquake (2007). High-resolution aftershock observations in the source region of the 2004 mid-Niigata Prefecture earthquake. *Earth, Planets and Space*, 59, 923–928.
- Kato, A., and group for the aftershock observations of the 2007 Niigataken Chuetsu-oki Earthquake (2008a). Imaging heterogeneous velocity structures and complex aftershock distributions in the source region of the 2007 Niigataken Chuetsu-oki Earthquake by a dense seismic observation. *Earth, Planets and Space*, 60, 1111–1116.
- Kato, A., and group for the aftershock observations of the 2007 Noto Hanto Earthquake (2008b). Three-dimensional velocity structure in the source region of the Noto Hanto earthquake in 2007 imaged by a dense seismic observation. *Earth, Planets and Space*, 60, 105–110.
- Kato, A., Sakai, S., Hirata, N., *et al.* (2006a). Imaging the seismic structure and stress field in the source region of the 2004 mid-Niigata Prefecture earthquake: structural zones of weakness, seismogenic stress concentration by ductile flow. *Journal of Geophysical Research*, 111, B08308, doi:10.1029/2005JB004016.
- Kato, A., Kurashimo, E., Igarashi, T., *et al.* (2009). Reactivation of ancient rift systems triggers devastating intraplate earthquakes. *Geophysical Research Letters*, 36, L05301, doi:10.1029/2008GL036450.
- Kato, A., Miyatake, T., and Hirata, N. (2010a). Asperity and barriers of the 2004 Mid-Niigata Prefecture earthquake revealed by highly dense seismic observations. *Bulletin of the Seismological Society of America*, 100(1), 298–306, doi:10.1785/0120090218.
- Kato, A., Iidaka, T., Iwasaki, T., Hirata, N., and Nakagawa, S. (2010b). Reactivations of boundary faults within a buried ancient rift system by ductile creeping of weak shear zones in the overpressured lower crust: the 2004 mid-Niigata Prefecture earthquake. *Tectonophysics*, 486, 101–107.
- Kato, A., *et al.* (2011). Anomalous depth dependency of the stress field in the 2007 Noto Hanto, Japan, earthquake: potential involvement of a deep fluid reservoir. *Geophysical Research Letters*, 38, L06306, doi:10.1029/2010GL046413.
- Kato, N., Sato, H., and Umino, N. (2006b). Fault reactivation and active tectonics on the fore-arc side of the back-arc rift system, NE Japan. *Journal of Structural Geology*, 28, 2011–2022.
- Kenner, S. J., and Segall, P. (2000). A mechanical model for intraplate earthquakes; application to the New Madrid seismic zone. *Science*, 289, 2329–2332.
- Loveless, J. P., and Meade, B. J. (2010). Geodetic imaging of plate motions, slip rates, and partitioning of deformation in Japan. *Journal of Geophysical Research*, 115, B02410, doi:10.1029/2008JB006248.
- Maruyama, T., Fusejima, Y., Yoshioka, T., Awata, Y., and Matsu'ura, T. (2005). Characteristics of the surface rupture associated with the 2004 Mid Niigata Prefecture earthquake, central Japan and their seismotectonic implications. *Earth, Planets and Space*, 57, 521–526.
- Michael, A. J., and Eberhart-Phillips, D. (1991). Relations among fault behavior, subsurface geology, and three-dimensional velocity models. *Science*, 253, 651–654.
- Miller, S. A., Collettini, C., Chiaraluce, L., *et al.* (2004). Aftershocks driven by a high-pressure CO₂ source at depth. *Nature*, 427, 724–727, doi:10.1038/nature02251.

- Nakajima, J., and Hasegawa, A. (2008). Existence of low-velocity zones under the source areas of the 2004 Niigata-Chuetsu and 2007 Niigata-Chuetsu-Oki earthquakes inferred from travel-time tomography. *Earth, Planets and Space*, 60, 1127–1130.
- Nishimura, T., Tobita, M., Yarai, H., et al. (2008). Episodic growth of fault-related fold in northern Japan observed by SAR interferometry. *Geophysical Research Letters*, 35, L13301, doi:10.1029/2008GL034337.
- Obara, K., Kasahara, K., Hori, S., and Okada, Y. (2005). A densely distributed high-sensitivity seismograph network in Japan: Hi-net by National Research Institute for Earth Science and Disaster Prevention. *Review of Scientific Instruments*, 76, 021301, doi:10.1063/1.1854197.
- Okada, T., Hasegawa, A., Suganomata, J., et al. (2007). Imaging the heterogeneous source area of the 2003 M6.4 northern Miyagi earthquake, NE Japan, by double-difference tomography. *Tectonophysics*, 430, 67–81.
- Okada, T., Umino, N., and Hasegawa, A. (2010). Deep structure of the Ou mountain range strain concentration zone and the focal area of the 2008 Iwate-Miyagi Nairiku earthquake, NE Japan: Seismogenesis related with magma and crustal fluid. *Earth, Planets and Space*, 62, 347–352.
- Okada, T., and group for the aftershock observations of the Iwate-Miyagi Nairiku Earthquake in 2008 (2012). *Earth, Planets and Space*, 64, 717–728.
- Okamura, Y., Ishiyama, T., and Yanagisawa, Y. (2007). Fault-related folds above the source fault of the 2004 mid-Niigata Prefecture earthquake, in a fold-and-thrust belt caused by basin inversion along the eastern margin of the Japan Sea. *Journal of Geophysical Research*, 112, B03S08, doi:10.1029/2006JB004320.
- Ozawa, S., Yarai, H., Tobita, M., Une, H., and Nishimura, T. (2008). Crustal deformation associated with the Noto Hanto earthquake in 2007 in Japan. *Earth, Planets and Space*, 60, 95–98.
- Sagiya, T., Miyazaki, S., and Tada, T. (2000). Continuous GPS array and present-day crustal deformation of Japan. *Pure and Applied Geophysics*, 157, 2303–2322.
- Sakai, S., and the group for the joint aftershock observation of the 2007 Noto Hanto Earthquake (2008). Highly resolved distribution of aftershocks of the 2007 Noto Hanto earthquake by a dense seismic observation. *Earth, Planets and Space*, 60, 83–88.
- Sato, H. (1994). The relationship between late Cenozoic tectonic events and stress field and basin development in northeast Japan. *Journal of Geophysical Research*, 99, 22261–22274.
- Sato, H., and Kato, N. (2005). Relationship between geologic structure and the source fault of the 2004 mid-Niigata Prefecture earthquake, central Japan. *Earth, Planets and Space*, 57, 453–457.
- Shibazaki, B., and Kato, A. (2012). Modeling the development of a complex fault configuration in the source region of two destructive intraplate earthquakes in the mid-Niigata region. *Tectonophysics*, 562–563, 26–33, doi:10.1016/j.tecto.2012.06.046.
- Shimazu, M., Yoon, S., and Takeishi, M. (1990). Tectonics and volcanism in the Sado-Pohang Belt from 20 to 14 Ma and opening of the Yamato Basin of the Japan Sea. *Tectonophysics*, 181, 321–330.
- Shinohara, M., Kanazawa, T., Yamada, T., et al. (2008). Fault geometry of 2007 Chuetsu-oki Earthquake inferred from aftershock distribution by ocean bottom seismometer network. *Earth, Planets and Space*, 60, 1121–1126.
- Sibson, R. H. (2007). An episode of fault-valve behaviour during compressional inversion? The 2004 MJ6.8 Mid-Niigata Prefecture, Japan, earthquake sequence. *Earth and Planetary Science Letters*, 257, 188–199.

- Takei, Y. (2002). Effect of pore geometry on VP/VS: from equilibrium geometry to crack. *Journal of Geophysical Research*, 107(B2), 2043, doi:10.1029/2001JB000522.
- Takenaka, H., Yamamoto, Y., and Yamasaki, H. (2009). Rupture process at the beginning of the 2007 Chuetsu-oki, Niigata, Japan, earthquake. *Earth, Planets and Space*, 61, 279–283.
- Terakawa, T., and Matsu'ura, M. (2010). The 3-D tectonic stress fields in and around Japan inverted from centroid moment tensor data of seismic events. *Tectonics*, 29, TC6008, doi:10.1029/2009TC002626.
- The Japanese University Group of the Joint Seismic Observations at NKTZ (2005). The Japanese University Joint Seismic Observations at the Niigata-Kobe Tectonic Zone (in Japanese with English abstract), *Bulletin of the Earthquake Research Institute, University of Tokyo*, 80, 133–147.
- Townend, J., and Zoback, M. D. (2006). Stress, strain, and mountain building in central Japan. *Journal of Geophysical Research*, 111, B03411, doi:10.1029/2005JB003759.
- Usami, T. (2003). *Materials for Comprehensive List of Destructive Earthquakes in Japan*. University of Tokyo Press (in Japanese).
- Uyeshima, M., Ogawa, Y., Honkura, Y., et al. (2005). Resistivity imaging across the source region of the 2004 Mid-Niigata Prefecture earthquake (M6.8), central Japan. *Earth, Planets and Space*, 57, 441–446.
- White, R. S., and the iSMM Team (2008). Lower-crustal intrusion on the North Atlantic continental margin. *Nature*, 452, 460–464.
- Williams, G. D., Powell, C. M., and Cooper, M. A. (1989). Geometry and kinematics of inversion tectonics. In *Inversion Tectonics*, ed. M. A. Cooper and G. D. Williams, Geological Society, London, Special Publication 44, pp. 3–15.
- Yoshimura, R., Oshiman, N., Uyeshima, M., et al. (2008). Magnetotelluric observations around the focal region of the 2007 Noto Hanto earthquake (Mj 6.9), central Japan. *Earth, Planets and Space*, 60, 117–122.
- Zhang, H., and Thurber, C. H. (2003). Double-difference tomography: the method and its application to the Hayward fault, California. *Bulletin of the Seismological Society of America*, 93, 1875–1889.
- Zhang, Q., Sandvol, E., and Liu, M. (2009). Lithospheric velocity structure of the New Madrid Seismic Zone: a joint teleseismic and local P tomographic study. *Geophysical Research Letters*, 36, L11305, doi:10.1029/2009GL037687.
- Zhao, D., Huang, Z., Umino, N., Hasegawa, A., and Kanamori, H. (2011). Structural heterogeneity in the megathrust zone and mechanism of the 2011 Tohoku-Oki earthquake (M_w 9.0). *Geophysical Research Letters*, 38, L17308, doi:10.1029/2011GL048408.